Journal of Applied Polymer Science

Preparation, characterization, and dynamic adsorption-desorption studies on polypyrrole encapsulated TiO_2 nanoparticles

Adil Sultan, Tarique Anwer, Sharique Ahmad, Faiz Mohammad
Department of Applied Chemistry, Faculty of Engineering and Technology, Aligarh Muslim University, Aligarh, 202002, India
Correspondence to: F. Mohammad (E-mail: faizmohammad54@rediffmail.com)

ABSTRACT: Binary doped polypyrrole (PPy) encapsulated Titania (TiO_2) nanoparticles were prepared by oxidative polymerization using $FeCl_3$ as oxidant in presence of camphorsulfonic acid (CSA) as surfactant. Both $FeCl_3$ (oxidant) and camphorsulfonic acid (surfactant) also act as dopant and hence thus prepared polypyrrole/Titania (TiO_2@PPy) is termed as binary doped nanocomposite i.e. $FeCl_3$ dopes polypyrrole by oxidation mechanism while camphorsulfonic acid dopes polypyrrole by protonic doping mechanism. The TiO_2@PPy coreshell nanocomposites were characterized by Fourier transform infrared spectroscopy (FTIR), X-ray diffraction (XRD), thermogravimetry, differential scanning calorimetry (DSC), field emission-scanning electron microscopy (FE-SEM), and inductance-capacitance-resistance (LCR) measurements. The results indicated that the structural and electrical properties of the TiO_2@PPy coreshell nanocomposites were significantly influenced by the extent of TiO_2 nanoparticles loading of polypyrrole. The direct current (DC) electrical conductivity of the as-prepared TiO_2@PPy coreshell nanocomposites was higher than that of PPy. As-prepared TiO_2@PPy coreshell nanocomposites were also studied for their dielectric losses for alternating current (AC) which is useful characteristic for their application in the fabrication of charge storing devices. TiO_2@PPy coreshell nanocomposites showed synergistic effect of combining components in improving their alcohol sensing properties. This improvement may be attributed to the adsorption on and desorption from alcohols TiO_2@PPy interface of the nanocomposites and alcohol vapors causing decrease in depletion region. The TiO_2@PPy coreshell nanocomposites were observed to show better reproducibility of electrical conductivity and fast self-recovery during the alcohol vapor sensing process. © 2016 Wiley Periodicals, Inc. J. Appl. Polym. Sci. **2016**, *133*, 43411.

KEYWORDS: addition polymerization; conducting polymers; properties and characterization

Received 9 October 2015; accepted 3 January 2016
DOI: 10.1002/app.43411

INTRODUCTION

The continuous rising interest in conducting polymer nanocomposites is due to their perceived potential applications in various fields such as batteries,[1] sensors,[2] electrochromic displays,[3,4] and so on. Like polymers in general, the conducting polymers are also lightweight and processible besides having tailorable electrical and electronic properties. Conducting polymers have received much attention after the first report of electrical conductivity in a conjugated polymer, polyacetylene, in 1977 by Shirakawa *et al.*[5] They combine the electrical and electronic properties of metals and semiconductors along with the advantages of polymers.[6] Because of the facile preparation,[7] easy control of the properties, good environmental stability, flexibility, and high electrical conductivity, polypyrrole is perceived to be one of the most promising conducting polymers for commercial applications.[8] Besides their high absorption coefficients in the visible region, conjugated polymers also exhibit high mobility of charge carriers as well as biocompatibility.[9]

Titania or titanium dioxide (TiO_2) is one of the most commonly used metal oxide semiconductors for photoinduced processes because of its comparatively low cost, low toxicity, and ability to resist photocorrosion. Different strategies have been developed to tune the band gap response of Titania to the visible region as the large band gap (~3.2 eV for anatase and brookite, ~3.0 eV for rutile) allows the utilization of only ~5% of the solar light. The strategies adopted include coupling of TiO_2 with narrow band gap semiconductors, doping with metal ion/non-metal ions and co-doping with two or more ions.[10] Nanosized TiO_2 has proven to be an efficient material for use in photocatalytic removal of hazardous industrial by-products and for photocatalytic water splitting. By inserting electrons into the conduction band of TiO_2 from conductive polymers with extending π-conjugated electron systems such as polyaniline, polythiophene, polypyrrole, and their derivatives, thus produced composites acts as stable photosensitizers.[11–13]

The preparation of nanocomposite particles with adjustable size constitutes a research area of considerable interest. Development

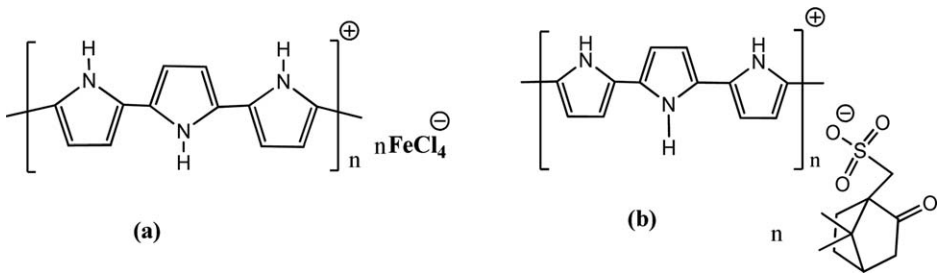

Figure 1. Schematic presentation of binary doping of polypyrrole by (a) $FeCl_3$ and (b) CSA.

of organic–inorganic nanocomposite materials have been regarded as an exciting class of materials as many bulk properties can be improved by this technique.[14] The combination of conducting polymer with the nanoparticles of oxide core material has led to exciting applications in photovoltaics,[15–18] magnetics,[19–21] charge storage,[22–25] catalysis,[26–28] biosensors,[29,30] and biomedicine,[31,32] which in turn has led to the development of newer original synthesis methodologies. In most cases, such nanocomposites are formed by electrochemical[33,34] or chemical polymerization[35,36] of monomer in presence nanosized oxide particles.

In this study, binary doped polypyrrole (PPy) and polypyrrole/Titania (TiO_2@PPy) coreshell nanocomposites with different amount of loading of TiO_2 nanoparticles were prepared via oxidative polymerization using $FeCl_3$ as an oxidant and camphorsulfonic acid (CSA) as surfactant. $FeCl_3$ dopes polypyrrole by oxidation mechanism while camphorsulfonic acid dopes polypyrrole by protonic doping mechanism. The effect of the enwrapping of TiO_2 nanoparticles (cloud shaped and spheres) by polypyrrole and the TiO_2 nanoparticles loading level in nanocomposites on the physicochemical properties was investigated. The morphology, thermal stability, and electrical conductivity of the resulting TiO_2@PPy coreshell nanocomposites were also investigated. These surface engineered products were analyzed for their dynamic response of electrical conductivity towards exposure to different types of alcohols by using 4-in-line-probe direct current (DC) electrical conductivity measurement set up.

EXPERIMENTAL

Materials

Pyrrole 99% (Spectrochem, India), anhydrous ferric chloride (Fisher Scientific, India), titanium dioxide 50 nm (MK Nano Canada), camphorsulfonic acid (CSA) (TCI, Tokyo), and methanol (E. Merck, India) were used as received. The water used in these experiments was double distilled.

Preparation of PPy and TiO_2@PPy Nanocomposites

Polypyrrole and polypyrrole/TiO_2 nanocomposites were prepared by oxidation of pyrrole in aqueous medium using $FeCl_3$ as an oxidant and CSA as surfactant. PPy was synthesized by oxidative polymerization method. Pyrrole (0.05 mol) and camphorsulfonic acid (0.01 mol) in 100 mL of distilled water were mixed. A solution of ferric chloride (0.05 mol) in 100 mL distilled water was then poured dropwise into the aqueous suspension of pyrrole/CSA. The reaction mixture was then stirred continuously for about 20 h, which resulted into the formation of black colored slurry. The product thus formed was filtered and washed several times with distilled water followed by methanol, dried in an air oven at 80 °C for 6 h, and stored in a desiccator for further experimentation.

Likewise, binary doped TiO_2@PPy coreshell nanocomposites (polypyrrole encapsulated TiO_2 nanoparticles) were prepared using the method described above while different amounts ultra-sonicated TiO_2 nanoparticles were added to reaction mixture as shown in Figure 1. As prepared materials were washed, dried, converted to fine powder, and stored in a desiccator for further analysis. Thus prepared material were designated as PPy, TiO_2@PPy-10, TiO_2@PPy-20, and TiO_2@PPy-30 containing 0%, 10%, 20%, and 30% of TiO_2 w/w of pyrrole in the reaction mixture, respectively. For electrical conductivity measurements, 0.30 g of each sample was pelletized at room temperature with the help of a hydraulic pressure instrument at 100 kN pressure applied for 15 min.

Characterization

The Fourier transform infrared spectroscopy (FTIR) spectra were recorded using Perkin-Elmer 1725 instrument on KBr pallets. To study the surface morphology, the field emission-scanning electron microscopy (FE-SEM) was done using LEO 435-VF microscope. X-ray diffraction (XRD) data were recorded by Bruker D8 diffractometer with Cu Kα radiation at 1.540 A° in the range of $5° \leq 2\theta \leq 70°$ at 40 kV. PPy and TiO_2@PPy coreshell nanocomposites were studied in terms of DC electrical conductivity by using a four-in-line probe with a temperature controller (PID-200, Scientific Equipments, Roorkee, India). The DC electrical conductivity was calculated by using the equation:

$$\sigma = \left[\ln 2\left(\frac{2S}{W}\right)\right] \Big/ \left[2\pi S\left(\frac{V}{I}\right)\right] \quad (1)$$

where I, V, W, and S are the current (A), voltage (V), thickness of the pellet (cm), and probe spacing (cm), respectively, and σ is the conductivity (S/cm).[37] Inductance-capacitance-resistance (LCR) properties were studied only PPy and TiO_2@PPy-20. For dynamic adsorption-desorption studies, these pellets were exposed to alcohol vapors and the response in term of electrical conductivity change was investigated to distinguish different types of alcohols.

RESULTS AND DISCUSSION

Oxidative Polymerization of Pyrrole by $FeCl_3$ and Doping

Binary doped polypyrrole was prepared by chemical oxidation of pyrrole in aqueous medium using $FeCl_3$ as an oxidant and CSA as surfactant as shown in eq. (2), Figure 1.

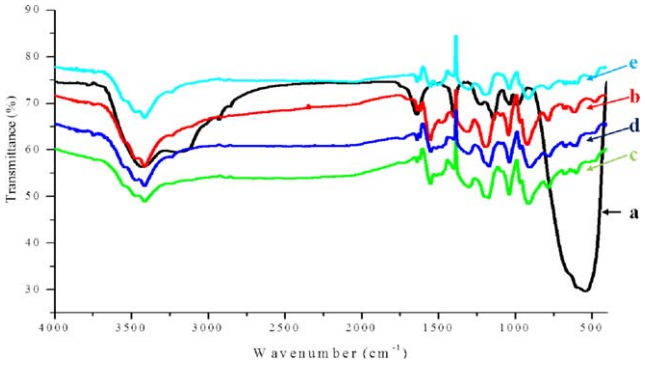

Figure 2. FTIR spectra of (a) as received TiO_2, (b) PPy, (c) TiO_2@PPy-10, (d) TiO_2@PPy-20, and (e) TiO_2@PPy-30. [Color figure can be viewed in the online issue, which is available at wileyonlinelibrary.com.]

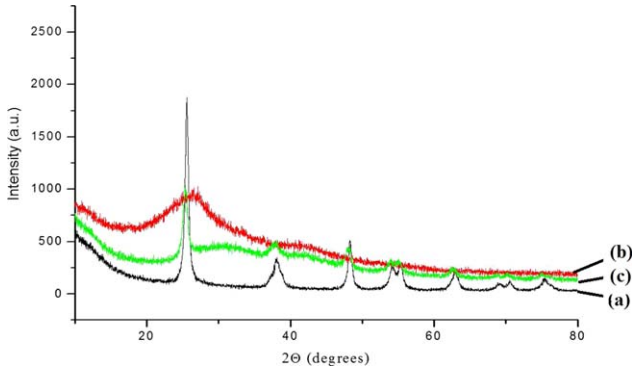

Figure 3. XRD patterns of (a) TiO_2, (b) PPy, and (c) TiO_2@PPy-20. [Color figure can be viewed in the online issue, which is available at wileyonlinelibrary.com.]

$$nPy + 2n\,FeCl_3 \rightarrow n\,FeCl_2 + n\,\overset{\oplus}{PPy}:\overset{(-)}{FeCl_4}. \quad (2)$$

FTIR Spectroscopic Study

In the FTIR spectrum of PPy, the main absorption peak was observed at 3412 cm^{-1} corresponding to stretching vibration of N–H bond as shown in Figure 2. The characteristic absorption bands for C=C, C=N, C–N stretching frequencies were observed at 1551, 1306, and 1189 cm^{-1}, respectively.[38] In case of TiO_2@PPy coreshell nanocomposites, the N–H, C=C, and C=N stretching frequencies were slightly shifted and were observed at 3419, 1562, and 1294 cm^{-1}, respectively. In addition to this, the band at 1201 cm^{-1} correspond to C–N$^+$ stretching and the band at ~916 cm^{-1} correspond to C=N$^+$–C stretching which are attributed to formation of bipolarons, which evidently support their doping by $FeCl_3$. It also suggest that polypyrrole was oxidized by $FeCl_3$, containing positively charged entities.[39] The slight increase in the N–H, C=C, C=N, and C–N stretching frequencies may probably be attributed to the interaction of PPy with TiO_2 nanoparticles. Although, the stretching frequencies corresponding to N–H bond of PPy were slightly different from those of TiO_2@PPy but their bending frequencies were observed to be similar and were approximately seen at 1050 cm^{-1}. The prominent absorption band of CSA may be seen at 1644 cm^{-1} supporting[40] its presence in PPy and TiO_2@PPy coreshell nanocomposites.

X-ray Diffraction (XRD) Analysis

The XRD patterns of the as-prepared PPy and TiO_2@PPy-20 coreshell nanocomposites are shown in Figure 3. A characteristic broad peak of PPy is centered at 26.65°, which may be assigned to the repeating units of pyrrole ring implying that the PPy is amorphous. These results are also consistent with the PPy obtained from conventional chemical or electrochemical methods.[41] In XRD pattern of TiO_2 nanoparticles, the characteristics peaks were observed at 2 θ= 25.50°, 37.17°, 48.33°, 53.98°, 55.50°, 63.27°, 68.92°, 70.71°, and 75.20° corresponding to (101), (004), (200), (105), (211), (204), (116), (220), and (215) planes, respectively.[42] In TiO_2@PPy-20 coreshell nanocomposite, the peaks of TiO_2 observed are comparatively weaker along with a broad peak of PPy that indicates the formation of the TiO_2@PPy coreshell nanocomposite. The XRD results show that the peak corresponding to PPy in the XRD pattern of TiO_2@PPy-20 coreshell nanocomposite is sharper than that in PPy indicating higher degree of crystallinity of TiO_2@PPy-20. This may be attributed to the filling of voids present in the polypyrrole matrix by TiO_2 nanoparticles, resulting a more ordered growth of PPy.

Thermogravimetric Analysis (TGA)

The thermogravimetric analysis (TGA) of PPy and TiO_2@PPy coreshell nanocomposites are shown in Figure 4. The amount of weight loss and thermal stability of the PPy and TiO_2@PPy coreshell nanocomposites were determined by means of TGA in the range of 40–800 °C. It may be observed that the initial weight loss below 150 °C for PPy may be attributed to the volatilization of water and oligomers. Second weight loss observed from 151 °C to 400 °C seems to be due to the degradation and volatilization of camphorsulfonic acid. The melting point of camphorsulfonic acid melts and volatilizes at 195 °C. The third weight loss observed from 401 °C to 700 °C seems to be due to the oxidative degradation of TiO_2 stabilized polypyrrole nanocomposites. Camphorsulfonic acid stabilizes polypyrrole to a great extent as has also been observed by Shubhra *et al.*[43] They observed a maximum weight loss of ~70% in the polypyrrole doped with camphorsulfonic acid similar to our findings. However, the PPy and TiO_2@PPy-20 coreshell nanocomposites show a minor weight loss throughout the temperature range

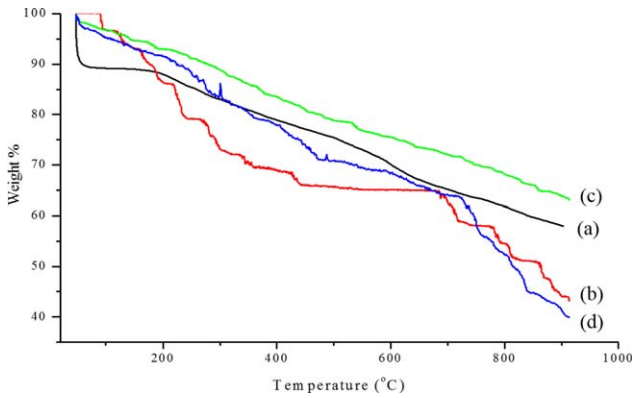

Figure 4. TGA thermograms of (a) PPy, (b) TiO_2@PPy-10, (c) TiO_2@PPy-20, and (d) TiO_2@PPy-30. [Color figure can be viewed in the online issue, which is available at wileyonlinelibrary.com.]

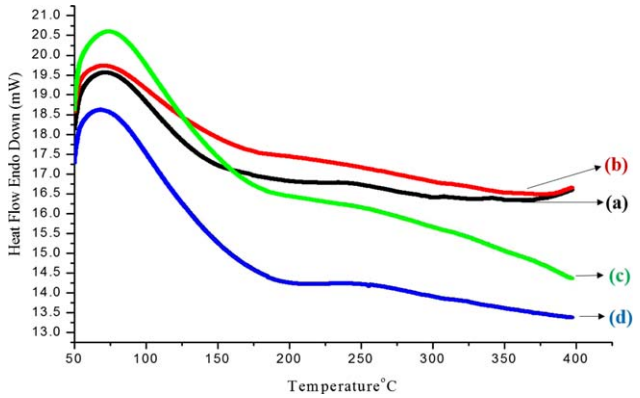

Figure 5. DSC thermograms of (a) PPy, (b) TiO_2@PPy-10, (c) TiO_2@PPy-20, and (d) TiO_2@PPy-30. [Color figure can be viewed in the online issue, which is available at wileyonlinelibrary.com.]

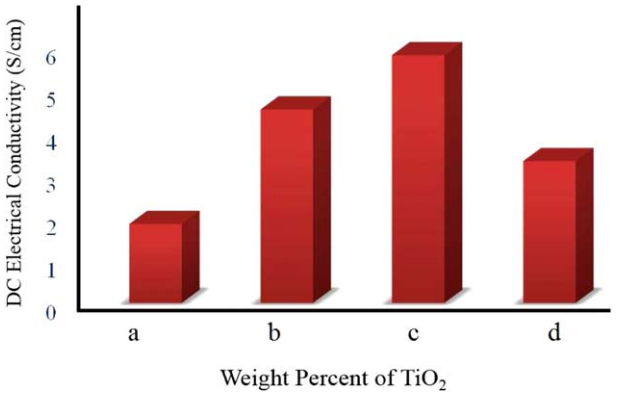

Figure 7. Initial DC Electrical conductivities of as-prepared (a) PPy, (b) TiO_2@PPy-10, (c) TiO_2@PPy-20, and (d) TiO_2@PPy-30. [Color figure can be viewed in the online issue, which is available at wileyonlinelibrary.com.]

indicating its higher thermal stability. In these cases, the dispersion of TiO_2 nanoparticles and CSA dopant in the nanocomposites plays an important role in changing the behavior of thermo oxidation. The improved thermal stability of TiO_2@PPy-20 coreshell nanocomposite is hence attributed to strong synergistic interaction between PPy and TiO_2 nanoparticles. As has been observed in other studies of these nanocomposites that the TiO_2@PPy-20 coreshell nanocomposite is the optimum composition for the formulation of a fairly good nanocomposite. It seems that there is some relation between the desirable properties including thermal stability of nanocomposites with the TiO_2 content in the nanocomposite formulations.

Differential Scanning Calorimetry (DSC)

Differential scanning calorimetry (DSC) was done to examine the changes in physical states of the samples, glass transitions in particular. The DSC thermograms of PPy and TiO_2@PPy coreshell nanocomposites are shown in Figure 5 in the temperature range of 50–400 °C. The DSC curve of PPy showed a broad endothermic dip at 143 °C, which can be attributed to the glass

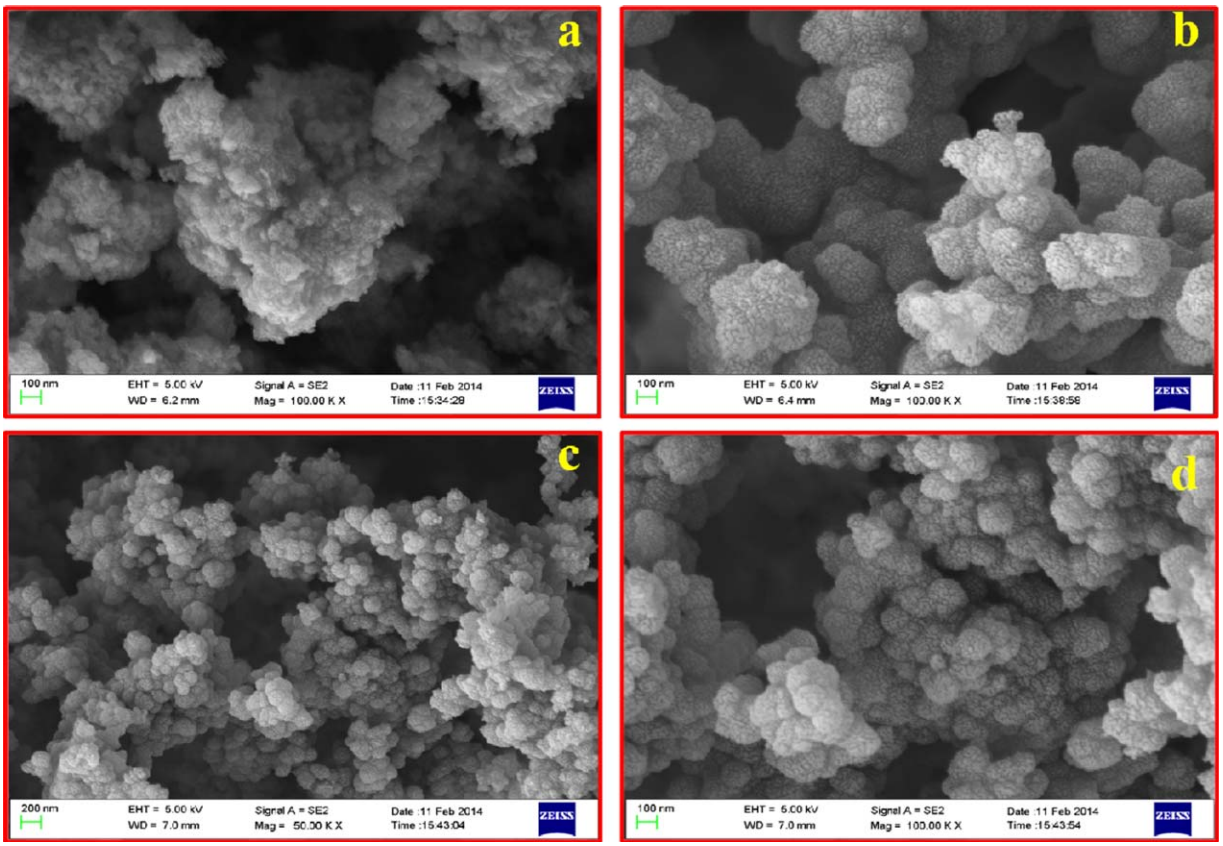

Figure 6. FE-SEM images of (a) TiO_2, (b) PPy, and (c,d) TiO_2@PPy-20 showing granular/spherical structure in two different magnifications. [Color figure can be viewed in the online issue, which is available at wileyonlinelibrary.com.]

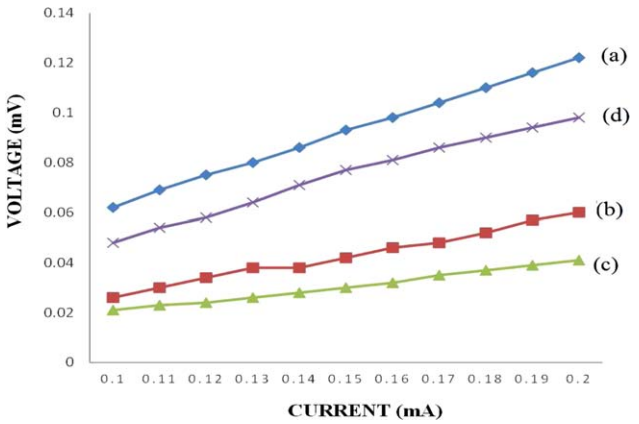

Figure 8. I–V characteristics of (a) PPy, (b) TiO_2@PPy-10, (c) TiO_2@PPy-20, and (d) TiO_2@PPy-30. [Color figure can be viewed in the online issue, which is available at wileyonlinelibrary.com.]

transition temperature of the polymer which was also perceived by Aliyeh *et al.*[44] The DSC plot of PPy further shows an inflection point at 370 °C, which can be attributed to the softening of PPy. The DSC graphs of TiO_2@PPy coreshell nanocomposites are shown in Figure 4(b–d). It was observed that the glass transition temperature increased from 171–197 °C with increase in TiO_2 content from 10 to 30%, which can be due to more ordered arrangement in the TiO_2@PPy coreshell nanocomposites as compared to PPy. It was also observed that the PPy with 10% TiO_2 content showed the inflection point at 380 °C and the inflection point around 380 °C disappears with further increase of TiO_2 content to 20% and 30%.

Scanning Electron Micrograph Studies

The morphology of PPy and TiO_2@PPy-20 coreshell nanocomposites were studied by FE-SEM and images are presented in Figure 6. The FE-SEM micrograph with high magnification [Figure 6(a)] clearly shows that the TiO_2 cluster exhibits a cloud-like structure comprised of spherical particles. The FESEM image of PPy is shown in Figure 5(b). It shows that the synthesized PPy is agglomerated by several nanoparticles. The as-prepared TiO_2@PPy-20 is composed of granules approximately of 100 − 200 nm in diameter [Figure 5(c,d)]. The granular/spherical structure of PPy is associated with the TiO_2 nanoparticles and CSA. The nanocomposites consisting of TiO_2 nanoparticles bind to the surface of large PPy polymer granules and their size remains unchanged due to the mild conditions of *in situ* polymerization. The TiO_2 nanoparticles are well dispersed in the nanocomposites. In these binary doped nanocomposites, no free TiO_2 nanoparticles in presence of CSA were observed which indicate that the TiO_2 nanoparticles and CSA have a nucleating effect on the pyrrole polymerization and caused a homogeneous PPy shell around them. FE-SEM study indicates the clear morphological transformations from PPy to TiO_2@PPy-20 coreshell nanocomposites.

DC Electrical Conductivity

The electrical conductivity (σ) and charge carriers are related by the expression:

$$\sigma = nq\mu \quad (3)$$

where n is number of charge carriers, q is the elementary charge (1.6×10^{-19} C), and μ is the charge carrier mobility.

The electrical conductivity of binary doped PPy and TiO_2@PPy coreshell nanocomposites with different amounts of TiO_2 measured by 4-in-line-probe method is comparable to those of polyaniline (emeraldine salt) and its nanocomposites with inorganic nanoparticles.[45] DC electrical conductivities of as-prepared PPy and TiO_2@PPy coreshell nanocomposites were observed to increase upto 20 wt % of TiO_2 loading followed by decrease in DC electrical conductivities on further loading to 30 wt % of TiO_2 as shown in Figure 7. The conductivity of PPy is 1.85 S/cm, which increases to 4.53 S/cm and 5.80 S/cm in the nanocomposites containing TiO_2 content 10 wt % and 20 wt % of pyrrole, respectively. With the further increase in TiO_2 content to 30 wt % of pyrrole, the conductivity decreased to 3.32 S/cm. This observed phenomenon is quite inconsistent with the results of most conducting composites combined with inorganic nanoparticles.[45] The presence of TiO_2 nanoparticles may induce the formation of more efficient network for charge transport in the

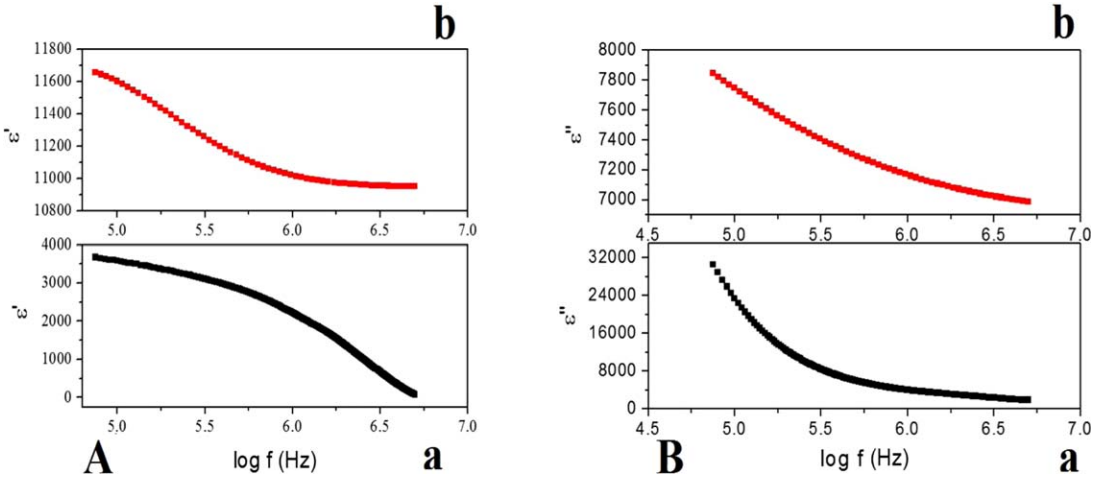

Figure 9. (A) Variation of real part of dielectric constants with frequency of (a) PPy and (b) TiO_2@PPy-20. (B) Variation of imaginary part of dielectric constants with frequency of (a) PPy and (b) TiO_2@PPy-20. [Color figure can be viewed in the online issue, which is available at wileyonlinelibrary.com.]

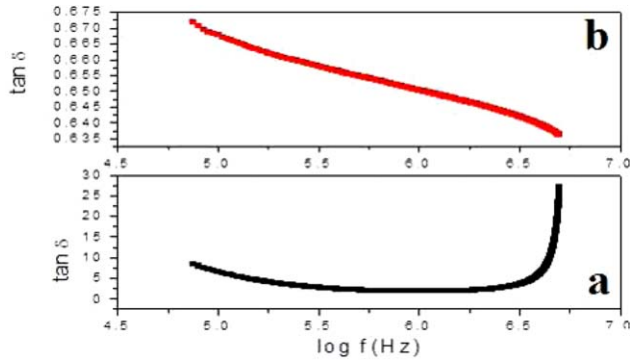

Figure 10. Variation of dielectric losses with frequency of (a) PPy and (b) TiO_2@PPy-20. [Color figure can be viewed in the online issue, which is available at wileyonlinelibrary.com.]

polypyrrole chains leading to higher conductivity. The reason for the increased conductivity may be associated with the increase in metallic regions in the nanocomposites, a reduction in tunneling/hopping distance between the metallic regions and the increased number of charge-carriers. The decrease in conductivity shown with the introduction of 30 wt % of TiO_2 nanoparticles in TiO_2@PPy-30 may be associated to the hindrance in the transport of carriers between different molecular chains of PPy due to increased Coulombic interactions leading to lower carrier mobility.

LCR Studies

I–V Studies. In the current–voltage graph shown in Figure 8, it may be observed that the highest voltage is shown by PPy at room temperature and at a particular current value. The voltage showed a decrease with the addition of 10 wt % and 20 wt % of TiO_2 content in the nanocomposites followed by an increase in voltage in case of TiO_2@PPy-30 at room temperature and at a particular current value. From this analysis, it may be inferred that the highest conductivity is shown by TiO_2@PPy-20 followed TiO_2@PPy-10 followed by TiO_2@PPy-30 followed by PPy as conductivity is inversely proportional to voltage. The characteristics of PPy and TiO_2@PPy nanocomposites showed ohmic variations, which are completely symmetrical with respect to the voltage. This linear increase in current with applied voltage is related to the conduction mechanisms of PPy and its nanocomposites. As the voltage increases, the formation of polarons and bipolarons increase rapidly contributing to higher values of current through the sample. The conduction in the metallic regions occurs by the hopping of charge carriers through the polaron structures that are formed after the binary doping of polypyrrole by $FeCl_3$ and CSA.

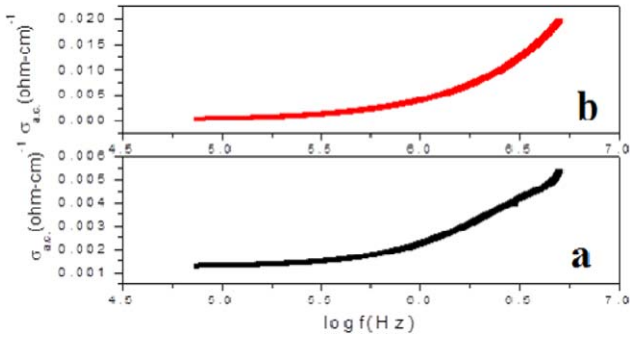

Figure 11. Variation of AC electrical conductivity with frequency of (a) PPy and (b) TiO_2@PPy-20. [Color figure can be viewed in the online issue, which is available at wileyonlinelibrary.com.]

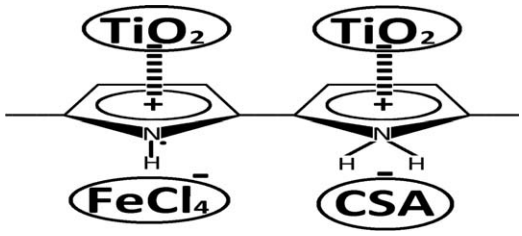

Figure 12. Interaction between TiO_2 nanoparticles and binary doped polypyrrole leading to the formation of nano p–n junctions.

Dielectric Constants. The dielectric constant is represented as $\varepsilon = \varepsilon' - j\varepsilon''$. The first term (the real part of the dielectric constant) describes the stored energy but the second term (imaginary part of the dielectric constant) describes the dissipated energy.[46] The dielectric constant of the samples (both the real, ε', and imaginary, ε'', parts) shows a sharp decrease at lower frequency and becomes almost constant or slowly decreases at higher frequency [Figure 9(A,B)]. Dielectric relaxation, a phenomenon that describes that the charge carrier localization is not stable and frequency disturbances that affect the charge carrier localization, can be the reason for the decrease in the dielectric constant with increasing frequency. The enhanced dielectric constant was observed for TiO_2@PPy-20 coreshell nanocomposite than PPy and it was also observed that dielectric constant increases with the addition of TiO_2 nanoparticles [Figure 9(A:a,b)]. This is attributable to accumulation of charge carriers in the internal surface of PPy matrix, which can be explained by Max-well–Wagner–Sillars effects.[46] The externally applied electric field incites the charge carriers that can migrate easily to the grains but these grains are accumulated at the boundaries, which in turn produce large polarization and high dielectric constant. In PPy and TiO_2@PPy-20, the high value of dielectric constants was observed at low frequency which can be attributed to the interfacial/space charge polarization TiO_2@PPy-20 coreshell nanocomposites. The polarization decreases with increase in frequency and then reaches a constant value due to the fact that beyond a certain frequency of external field, the hopping of electrons between metal ions and PPy cannot follow the alternating field. The increase in loading percent of TiO_2 nanoparticles in the TiO_2@PPy-20 coreshell nanocomposites results into the formation of many interfaces between PPy and TiO_2 nanoparticles that enhances the accumulation of charge carriers in the internal surface of the PPy matrix.[47]

Dielectric Losses. As shown by the analysis, the PPy and TiO_2@PPy-20 coreshell nanocomposite exhibited frequency dependent dielectric losses and they showed the uniform behavior of dielectric losses although PPy and TiO_2@PPy-20 coreshell nanocomposite at higher frequency (Figure 10). The amount of TiO_2 nanoparticles in TiO_2@PPy-20 coreshell nanocomposite

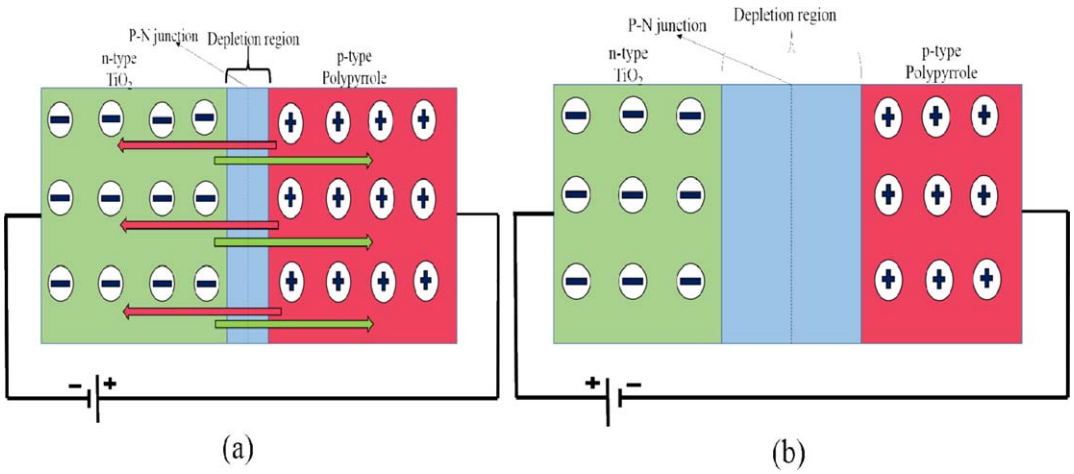

Figure 13. Schematic diagram of formation of nano p–n junctions in TiO_2@PPy (a) forward bias and (b) reverse bias. [Color figure can be viewed in the online issue, which is available at wileyonlinelibrary.com.]

affected the dielectric losses. The low value of dielectric losses at lower frequency may be attributable to the low resistivity caused by grain boundaries.[48] Moreover, the TiO_2@PPy-20 coreshell nanocomposite showed low dielectric losses than PPy which suggests the suitability of TiO_2@PPy-20 coreshell nanocomposite for the electronic applications in fabrication of capacitors.

Alternating Current (AC) Electrical Conductivity. Total electrical conductivity $\sigma tot = \sigma o(T) + t(\omega, T)$ is the summation of the band and hopping fractions. The first term is DC conductivity due to the band conduction, which is frequency independent. The second term is the pure alternating current (AC) conductivity due to the electron hopping processes.[49] AC conductivity of TiO_2@PPy-20 coreshell nanocomposite was found to be higher than that of PPy as shown in Figure 11. Its analysis showed that the AC conductivity of TiO_2@PPy-20 coreshell nanocomposite slowly increases with an increase in the frequency of AC field and increases rapidly at higher frequencies. The PPy shows a very slow increase in AC conductivity with increase in frequency even at high frequency as compared to TiO_2@PPy-20 coreshell nanocomposite which may be due to the increase in frequency leading to enhanced electronic exchange occurring among the cations with two and three valences existing in the sub-lattice of TiO_2 nanoparticles. An increase in AC conductivity was also observed with the loading of TiO_2 nanoparticles in TiO_2@PPy-20 coreshell nanocomposite. It was also observed that the presence of increased amounts of TiO_2 nanoparticles in the TiO_2@PPy-20 coreshell nanocomposite causes a more radical increment in the AC conductivity at high frequency, which may be attributed to the enhanced electron hopping phenomenon.[50]

Dynamic Absorption–Desorption Studies

In this proposed scheme, there are two types of electron transfers in the TiO_2@PPy coreshell nanocomposites. First electron transfer between PPy and $CSA/FeCl_3$ and second between the

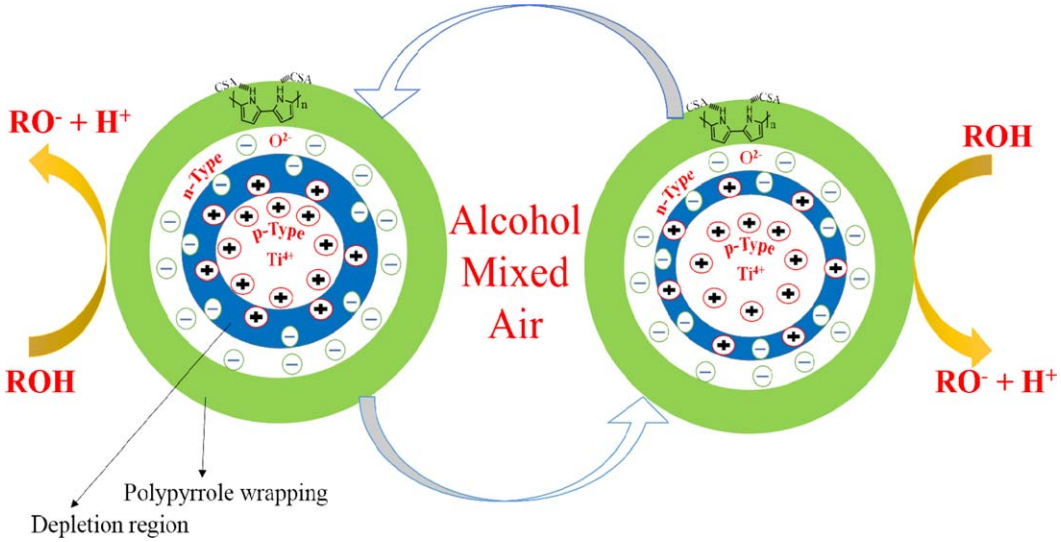

Scheme 1. Schematic presentation of alcohol sensing by TiO_2@PPy-20. [Color figure can be viewed in the online issue, which is available at wileyonlinelibrary.com.]

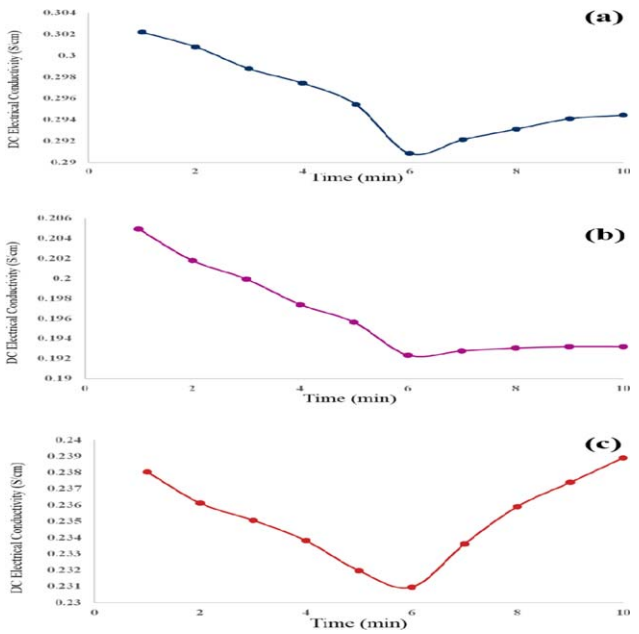

Figure 14. Effect on the DC electrical conductivity of PPy on exposure to (a) 1°, (b) 2°, and (c) 3° alcohols with respect to time. [Color figure can be viewed in the online issue, which is available at wileyonlinelibrary.com.]

PPy and TiO_2 (Figure 12). The DC electrical conductivity of TiO_2@PPy coreshell nanocomposites increased remarkably, which can be attributed to the doping effect associated with CSA, $FeCl_3$, and TiO_2, which induce the formation of more number of charge carriers. The DC electrical conductivity was found to increase with increasing contents of TiO_2 nanoparticles, which may be attributed to the increased mobility of charge carriers, which increases the hopping rate of charge carriers. Further increasing the content of TiO_2, it seems that the mobility of charge carriers decreases due to Columbic interactions, which leads to decrease in electrical conductivity. Therefore, the delocalization effect along with formation of polarons or bipolarons causes the enhancement of electrical conductivity.

Another explanation for decrease in electrical conductivity in case of TiO_2@PPy-30 may be given by effective p–n junction formation between PPy and TiO_2−30 as follows. Binary doped polypyrrole and TiO_2 nanoparticles are p-type and n-type semiconductors, respectively. When the TiO_2 nanoparticles are encapsulated by PPy, nano p–n junction regions are generated which leads to an increase in electrical conductivity as shown in Figure 13. Because of the forward bias, the holes in p-type region and electrons in n-type region are pressed towards the junction which leads to the increase in the number of holes, reduced width of depletion region and reduction in the negative charge at the junction. In 30 wt % TiO_2 content, the electrical conductivity decreases probably due to the generation of reverse bias. In the light of above discussion, the dynamic sorption–desorption of PPy and TiO_2@PPy-20 and its effect on electrical conductivity is explained.

The alcohols butan-1-ol (1° alcohol), butan-2-ol (2° alcohol), and 2-methyl propan-2-ol (3° alcohol) vapor sensitivity towards

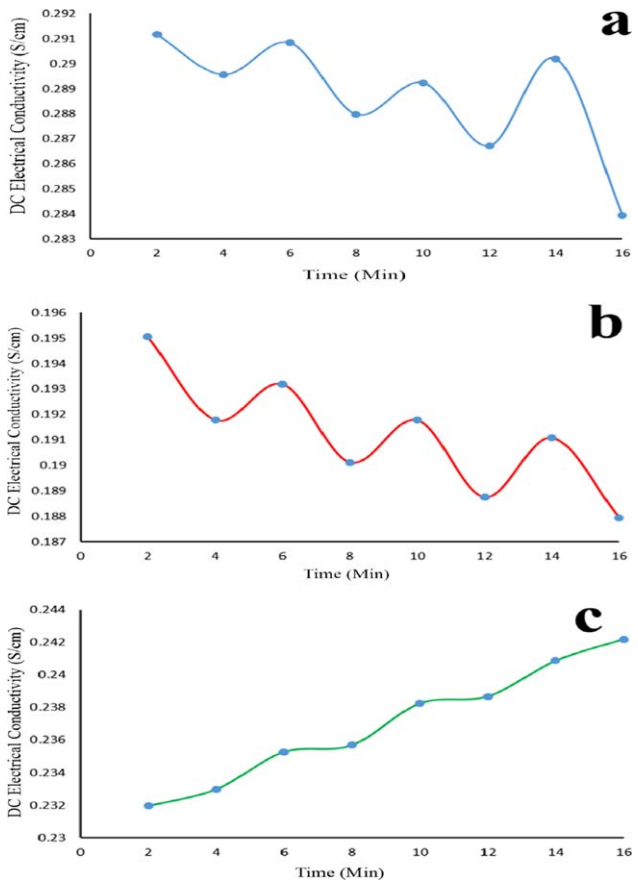

Figure 15. Variation in conductivity of (a) 1° alcohol, (b) 2° alcohol, and (c) 3° alcohol on PPy on alternating exposure to alcohols. [Color figure can be viewed in the online issue, which is available at wileyonlinelibrary.com.]

PPy was analyzed by measuring the changes in the electrical conductivity at room temperature (Scheme 1). The vapor sensitivity towards PPy was investigated based on two different factors, namely, the response time and the sensing intensity. The alcohol concentration in aqueous solutions used for these experiments was 1 *M*. The polypyrrole pellets were firstly exposed to alcohol vapors for 5 min and the exposed to air for another 5 min. When PPy was exposed to alcohol vapors, it was observed that the overall electrical conductivity decreases with time. Different types of alcohols showed different

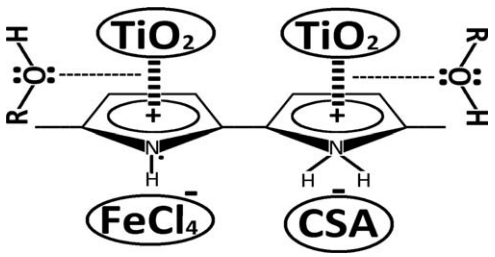

Scheme 2. Binary doped polypyrrole and TiO_2@PPy coreshell nanocomposites forming nano p–n junctions. ROH molecules interact at p–n nano junctions formed at TiO_2@PPy interface.

behaviors and it was observed that in case of 1° alcohol, the electrical conductivity decreased with increase in the time period. The 2° alcohol showed greater decrease in electrical conductivity as compared to the 1° alcohol. In case of 3° alcohol, the electrical conductivity increases in comparison to 2° alcohol but increase is less than that in 1° alcohol. The variation in electrical conductivity is attributed to the charge transfer between alcohol and polypyrrole. The sensitivity of polypyrrole and its nanocomposites towards alcohol vapor molecules is due to the adsorption of alcohol vapors on polypyrrole surface making an unstable complex, which in turn reduces the electrical conductivity. When the PPy pallet was taken out from the alcohol vapor (5–6 min), the conductivity decreased due to the adsorption of some of alcohol vapors over polypyrrole (Figure 14). However, after the sixth minute the electrical conductivity started to increase as the alcohol vapors started to desorb from polypyrrole. The following reversible adsorption/desorption may be suggested for their use in alcohol vapor sensing.

The reproducibility was measured by first keeping the sample in alcohol vapors for 2 min followed by 2 min in air (Figure 15). The 1° and 2° alcohols showed good reproducibility than 3° alcohol. The reason for the poor reproducibility shown by 3° alcohols may be attributed to the steric hindrance experienced by 3° alcohol to interact with PPy surface hence decrease in conductivity was least. On the other hand, 2° alcohol showed the higher reproducibility due to good adsorption and desorption.

The TiO_2@PPy-20 coreshell nanocomposite may be seen as one of the most favorable sensing materials due to its high alcohol vapor sensitivity at room temperature. Polypyrrole behaved as p-type semiconductor and TiO_2 as n-type semiconductor leading to the formation of large number of nano p–n junctions as shown in Scheme 2. When the composites were exposed to alcohol vapors that acted as electron donor, the depletion region changed and the electrical conductivity of conducting polymer increased continuously. Therefore, the width of the depletion region decreased and the conductivity of the polypyrrole channel increased, which was also observed by Patil and coworkers.[51]

Shaowei Chen and coworkers[52] observed that enhancement in charge carriers due to their interaction at molecular level with

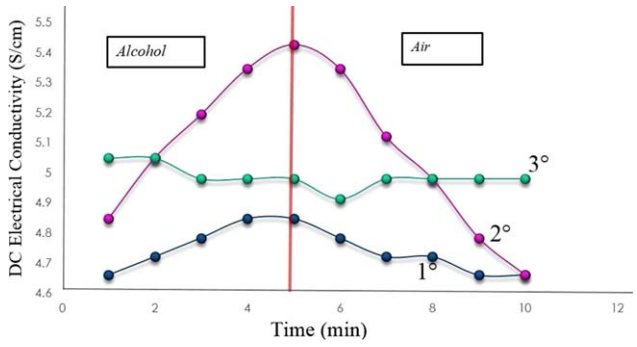

Figure 16. Effect on the conductivity of TiO_2@PPy-20 on exposure to different alcohols with respect to time. [Color figure can be viewed in the online issue, which is available at wileyonlinelibrary.com.]

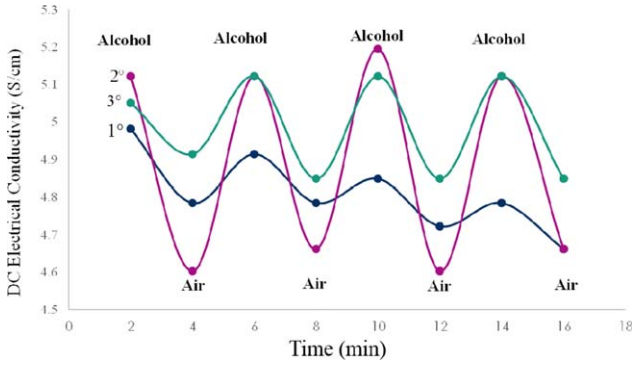

Figure 17. Variation in conductivity of TiO_2@PPy-20 on alternate exposure to alcohols. [Color figure can be viewed in the online issue, which is available at wileyonlinelibrary.com.]

the surface when TiO_2 nanoparticles were exposed to alcohol vapors. This ionic interaction decreased the thickness of depletion region, which brought them close to each other and thus enhanced the conductivity of TiO_2 nanoparticles.

Rajesh *et al.* suggested that ZnO nanostructures are considered as excellent material for fabrication of highly sensitive and selective gas sensors. They also discussed gas-sensing characteristics such as gas response, response time, recovery time, selectivity, detection limit, stability, and recyclability.[53]

The variation in electrical conductivity may be attributed to the number of charge carriers distributed between alcohol molecules and the TiO_2 nanoparticles encapsulated with polypyrrole. The sensitivity of polypyrrole towards alcohol molecules is due to the interaction of alcohol vapors on TiO_2@PPy-20 interface forming an unstable complex, which in turn raises the electrical conductivity. From the Figure 16, when the TiO_2@PPy-20 was taken out from the alcohol vapor the conductivity decrease due to desorption of alcohol vapors from the interface of TiO_2@PPy-20. The 2° alcohol showed maximum response towards TiO_2@PPy-20. The 1° and 3° alcohols showed comparatively poor response as evident from lower amplitude. The reproducibility of 1° and 3° alcohols is somewhat similar.

The reproducibility of response was measured by first keeping the sample in alcohol vapors for 2 min followed by 2 min in air as shown in Figure 17. The 2° alcohol showed the best reproducibility of response and highest amplitude. All the molecules of 2° alcohol adsorbed on the TiO_2@PPy-20 surface get desorbed on exposure to air, it may be suggested. The 1° and 3° alcohols showed at least same and good reproducibility than secondary alcohol. The reason for the least and almost equal reproducibility shown by primary and tertiary alcohols may be due to the less inductive effect (+I-effect) and steric hindrance, respectively. Quantitatively, both effects are of comparable extent and affects the adsorption of incoming molecules upto same degree resulting into almost same type of response. That's why lesser molecules of 1° and 3° alcohol are able to get adsorbed on the TiO_2@PPy-20 coreshell nanocomposite surface hence decrease in conductivity was least.

CONCLUSIONS

In summary, PPy and TiO_2@PPy coreshell nanocomposites were synthesized successfully via *in situ* polymerization method, which were confirmed through different instrumental techniques. We have presented a detailed study of electrical, dielectric, and sensing properties. The electrical properties presented in terms of DC electrical conductivity and I–V characteristics. The binary doped TiO_2@PPy-20 coreshell nanocomposite showed better electrical, dielectric, and sensing properties. Electrical conductivity studies showed the more efficient charge transport behavior and may be applied in diode properties. At this stage, we may suggest the formation of nano p–n junctions at the nanocomposite of TiO_2@PPy interface.

ACKNOWLEDGMENTS

Adil Sultan acknowledge with thanks the utmost support and thoughtful suggestions of Mr. Nayeem Ahmed.

REFERENCES

1. Kemp, N. T.; Flanagan, G. U.; Kaiser, A. B.; Trodahl, H. J.; Chapman, B.; Partridge, A. C.; Buckley, R. G. *Synth. Met.* **1999**, *101*, 434.
2. Skotheim, T. A. Handbook of Conducting Polymers; Marcel Dekker: New York, **1986**.
3. Skotheim, T. A.; Elsenbaumer, R.; Reynolds, J. Hand-Book of Conducting Polymers; Marcel Dekker: New York, **1998**.
4. Wallace, G. G.; Spinks, G.; Teasdale, P. R. Conductive Electroactive Polymers; Technomic: New York, **1997**.
5. Shirakawa, H.; Louis, E. J.; MacDiarmid, A. G.; Chiang, C. K.; Heeger, A. J. *J. Chem. Soc. Chem. Commun.* **1977**, *16*, 578.
6. Bakhshi, A. K.; Bhalla, G. *J. Sci. Ind. Res.* **2004**, *63*, 715.
7. Jurewicz, K.; Delpeux, S.; Bertagna, V.; Beguin, F.; Frackowiak, E. *Chem. Phys. Lett.* **2001**, *347*, 36.
8. Campbell, T. E.; Hodgson, A. J.; Wallace, G. G. *Electroanal.* **1999**, *11*, 215.
9. Patil, A. O.; Heeger, A. J.; Wudl, F. *Chem. Rev.* **1988**, *88*, 183.
10. Kumar, S. G.; Devi, L. G. *J. Phys. Chem. A* **2001**, *115*, 13211.
11. Roberson, L. B.; Poggi, M. A.; Kowalik, J.; Smestad, G. P.; Bottomley, L. A.; Tolbert, L. M. *Coordin. Chem. Rev.* **2004**, *248*, 1491.
12. Beek, W. J. E.; Wienk, M. M.; Kemerink, M.; Yang, X.; Janssen, R. A. J. *J. Phys. Chem. B* **2005**, *109*, 9505.
13. Min, S. X.; Wang, F.; Han, Y. Q. *J. Mater. Sci.* **2007**, *42*, 9966.
14. Novak, B. M. *Adv. Mater.* **1993**, *5*, 422.
15. Giraudeau, A.; Fan, F. R. F.; Bard, A. J. *J. Am. Chem. Soc.* **1980**, *102*, 5137.
16. Hagfeldt, A.; Gratzel, M. *Chem. Rev.* **1995**, *95*, 49.
17. Roux, S.; Soler, I. G. J. A.; Demoustier, C. A. A. S.; Sanchez, P. C. *Adv. Mater.* **2003**, *15*, 217.
18. Williams, E. L.; Jabbour, G. E.; Wang, Q.; Shaheen, S. E.; Ginley, D. S.; Schiff, E. A. *Appl. Phys. Lett.* **2005**, *87*, 223504.
19. Butterworth, M.; Armes, S. P.; Simpson, A. W. *J. Chem. Soc., Chem. Commun.* **1994**, *10*, 2129.
20. Philipse, A. P.; van Bruggen, M. P. B.; Pathmamamoharan, C. *Langmuir* **1994**, *10*, 92.
21. Nguyen, M. T.; Diaz, A. *Adv. Mater.* **1994**, *6*, 858.
22. Miyauchi, S. N.; Abiko, H.; Sorimachi, Y.; Tsubata, I. *J. Appl. Polym. Sci.* **1989**, *37*, 289.
23. Cantu, M. L.; Romero, P. G. *Chem. Mater.* **1998**, *10*, 698.
24. Kulesza, P. J.; Skunik, M.; Baranowska, B.; Miecznikowski, K.; Chojak, M.; Karnicka, K.; Frackowiak, E.; Beguin, F.; Kuhn, A.; Delville, M. H.; Starobrzynska, B.; Ernst, A. *Electrochim. Acta* **2006**, *51*, 2373.
25. Mallouki, M.; Tran-Van, F.; Sarrazin, C.; Simon, P.; Daffos, B.; De, A.; Chevrot, C.; Fauvarque, J. F. *J. Solid State Electrochem.* **2007**, *11*, 398.
26. Qi, Z.; Pickup, P. G. *Chem. Commun.* **1998**, *15*, 849.
27. Qi, Z.; Pickup, P. G. *Chem. Commun.* **1998**, 2299.
28. Park, J. E.; Atobe, M.; Fuchigami, T. *Electrochim. Acta* **2005**, *51*, 849.
29. Bharathi, S.; Nogami, M. *Analyst* **2001**, *1*, 1919.
30. Hamilton, S.; Hepher, M. J.; Sommerville, J. *Sens. Actuators, B* **2005**, *107*, 424.
31. Goodwin, J. W.; Habron, R. S.; Reynolds, P. A. *Colloid Polym. Sci.* **1990**, *268*, 766.
32. Chen, Y.; Chong, S. C. *J. Phys. Conference Series* **2006**, *34*, 204.
33. Okano, M.; Itoh, K.; Fujishima, A.; Hondo, K. *J. Electrochem. Soc.* **1987**, *134*, 837.
34. Yu, O.; Tan, Z.; Wang, F. *Chin. Chem. Lett.* **1991**, *2*, 471.
35. Rammelt, U.; Hebestreit, N.; Fikus, A.; Plieth, W. *Electrochim. Acta* **2001**, *46*, 2363.
36. Hebestreit, N.; Hofmann, J.; Rammelt, U.; Plieth, W. *Electrochim. Acta* **2003**, *48*, 1779.
37. Ansari, M. O.; Yadav, S. K.; Cho, J.; Mohammad, W. F. *Compos. B* **2013**, *47*, 155.
38. Tao, Y.; Enguo, J.; Jinsong, R.; Xiaogang, Q. *Chem. Commun.* **2014**, *50*, 3030.
39. Robison, B.; Fernández, M. J. G.; Mercedes, M. P. B.; Antonio, S. *Green Chem.* **2013**, *15*, 1981.
40. Jafarpour, M.; Ghahramaninezhad, M.; Rezaeifard, A. *New J. Chem.* **2014**, *38*, 2917.
41. Jang, J.; Yoon, H. *Langmuir* **2005**, *21*, 11484.
42. Shen, Y.; Wan, M. *J. Appl. Polym. Sci.* **1998**, *68*, 1277.
43. Shubhra, G.; Nasreen, A. M.; Alka, G. *Polym. Adv. Technol.* **2010**, *21*, 205.
44. Aliyeh, Y. A. M.; Hossien, E.; Zahra, T.; Marjan, T. *J. Eng. Sci. Technol.* **2012**, *7*, 5540.
45. Ansari, M. O.; Mohammad, F. *J. Appl. Polym. Sci.* **2012**, *124*, 4433.
46. Azam, A.; Ahmed, A. S.; Chaman, M.; Naqvi, A. H. *J. Appl. Phys.* **2010**, *108*, 94329.

47. Thomas, P. K.; Dwarakanath; Varma, K. B. R. *Synth. Met.* **2009**, *159*, 2128.

48. Dey, A.; De, S.; De, A.; De, S. K. *Nanotechnol.* **2004**, *15*, 1277.

49. Bhadra, S.; Singha, N. K.; Khastgir, D. *Curr. Appl. Phys.* **2009**, *9*, 396.

50. Ata, A. M.; Nimra, A. E.; El, M. K.; Attia, S. M.; Kony, D.; El, Al-Hammadi, A. H. *J. Magn. Magn. Mater.* **2006**, *33*, 297.

51. Chougule, M. A.; Dalavi, D. S.; Sawanta, M.; Patil, P. S.; Moholkar, A. V.; Agawane, G. L.; Kim, J. H Shashwati, S.; Patil, V. B. *Measurement* **2012**, *8*, 1989.

52. Peiguang, H.; Guojun, D. W.; Zhou, J.; Cui, J.; Lin, H.; Liu, D.; Liu, J. Wang, Chen, S. **2010**, *ACS Appl. Mater. Interfaces 2*, 3263.

53. Rajesh, K.; Al-Dossary, O.; Girish, K.; Ahmad, U. *Nano-Micro Lett.* **2015**, *7*, 97.